ACS APPLIED MATERIALS & INTERFACES

Research Article

www.acsami.org

Multifunctional Self-Healing and Self-Reporting Polymer Composite with Integrated Conductive Microwire Networks

Yan Hong[†,‡,*] and Ming Su[‡]

[†]Rheem Manufacturing Company, 2600 Gunter Park Drive East, Montgomery, Alabama 36109, United States

[‡]NanoScience Technology Center, University of Central Florida, Orlando, Florida 32826, United States

ABSTRACT: Electrically reported self-healing polymers are designed by mimicking skins of animal, and made by embedding an ordered network of glass microtubes inside polymer matrices. The microtubes contain metallic microwires, and mixtures of healing agent and conductive carbon powders. Cracks on the surface due to external forces or inside the polymer due to dislocation motions break glass microtubes, release healing agent with carbon powders. The percolations of electrons through released carbon powders to coordinately align conductive microwires report the locations of damages and healing events.

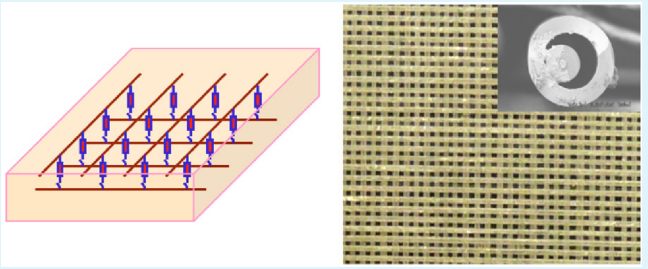

KEYWORDS: *self-healing polymer, self-reporting network, conductive microwires, fiber-drawing nanomanufacturing*

1. INTRODUCTION

Self-healing materials (i.e., polymers) are designed by mimicking the damage repairing abilities of biological systems (skin or bone).[1,2] In responses to external physical or mechanical stimuli, self-healing polymers can release healing agents in situ to repair microcracks produced by external mechanical forces or internal dislocation motions.[3−6] The healing agents are usually encapsulated in breakable microcapsules or microvascular networks of glasses or polymers, and applied as thin film coatings or embedded in the matrix of polymers.[7−9] Healing processes start from mixing of two reactive components through spontaneous diffusions, and are facilitated by external interventions in forms of heat treatment, pH or pressure changes.[9−13] Microtubes or microfabricated vascular structures can be used to deliver and replenish healing agents to achieve multiple healing cycles.[14−16] In several cases, the mechanical properties of the damaged polymers could be fully recovered or enhanced.[17,18] Upon the successful developments of many applicable self-healing polymer systems, the research interests have gradually shifted to achieve multifunctional polymers. One step further toward so-called "smart polymers" is the combination of self-healing ability with self-reporting ability. In nature, the self-healing processes of mammalian skins are uniquely integrated with self-reporting neuronal networks, which allow triggering a facilitated repairing process, and reporting damage/repair events and their locations, as well as the health status of structures over a large area.[19]

Achieving self-reporting and self-healing abilities in man-made material systems will enable a wide range of technological possibilities. The uncertainty associated with unexpected damage to polymer materials has been a major concern for applications where the structural integrity is of primary importance. For instance, the ability to self-repair damages and monitor the health status of critical parts will significantly improve reliability, and reduce maintenance costs in space and air transportation systems.[20] But, most of available techniques for structural monitoring have to be carried out on partially disassembled components, therefore it is hard to identify damages effectively and rapidly in real time. Although miniaturized transducers could be embedded in such critical components, there is a lack of connections between the measured signals and the health status of polymers. In addition, these microfabricated devices are often too complex and expensive to cover a surface area as large as an airplane wing at reasonable detection density (i.e., spatial resolution).[21] In the cases of self-healing polymers, there exists a larger uncertainty regarding the health status of polymer because of the unknown information on the locations, qualities of repaired microcracks and available amount of healing agents, etc. Although fluorescent dye molecules can be mixed with healing agents to form colored patches over damaged areas, this method will only report damage close to or on the surface of opaque parts during ground tests, and cannot detect microcracks inside the polymers in real time.[22]

We had worked on a fiber drawing nanomanufacturing (FDN) method to make ordered arrays of glass microstructures (i.e microspike, microchannel and microwell), glass encapsulated semiconductive and metallic micro/nanowires, and glass microtubes.[23−26] The similar method can be used to make metal encapsulated superconducting wires, nanocone array glass and nanochannel glass.[27−29] In this approach, Ultralong

Received: May 31, 2012
Accepted: July 2, 2012
Published: July 2, 2012

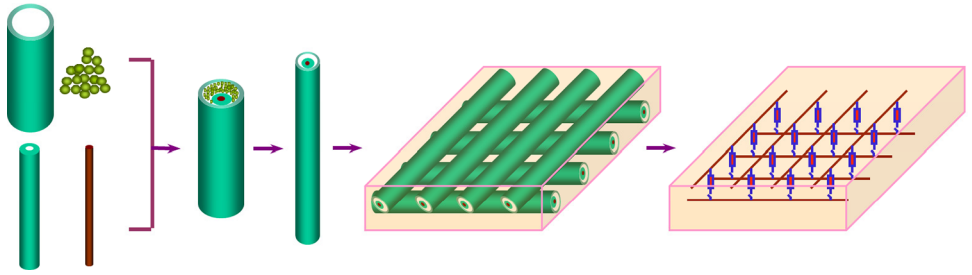

Figure 1. Self-reported self-healing polymer with fibrous building blocks.

conductive micro/nanowires and hollow microtubes have been fabricated through FDN process. The hollow glass microtubes are filled with conductive healing agent, and assembled to form ordered network, which can be embedded in a polymer matrix to achieve self-reported self-healing polymer that repairs damage by releasing conductive healing agent, and reports damage/repair event through the network of conductive microwires. This approach allows fabrications of polymers with enhanced reliability and structural integrity, and provides high resolution in detecting the mechanical damages to polymer composite.

2. EXPERIMENTAL SECTION

2.1. Fabrication of Integrated Microtubes. To integrate alloy micro/nanowires (as sensing material) and microtubes (as hosting structure) for healing agents to an ordered two-dimensional (2D) network, we have designed a multicomponent preform containing conductive alloy wires and tube-forming materials and salt powders, (salt powders), instead of using normal preform that has one type of filling material. The preform is formed by filling a copper-phosphor (the mass ratio of Cu−P of 92.7:7.3) alloy wire (Aldrich) into a Pyrex glass tube (Schott 8330). This commercially available Cu−P alloy wire has similar melting range as Pyrex glass (700−800 °C). The good electrical conductivity makes is a very good candidate as the 2D electrical network component. The glass tube is inserted into a second glass tube with larger inner diameter. The empty spaces between two glass tubes are filled with powders of sodium chloride (salt) (Figure 1). Then the preform is drawn to long microfibers with diameter of about 730 μm at 850 °C, followed by cutting microfibers into short pieces of equal length. The outer and inner diameters, and thicknesses of glass microtubes, as well as the diameter of alloy microwire are reduced from millimeters down to several hundred micrometers or smaller. The purpose of using the smaller diameter glass tube is to physically separate the alloy and salt powders which melt at approximately the same temperature. Although only touching each other in the preform, the two glass tubes melt and form stable connections at contact region even in the presence of molten salt. After cooling down to room temperature, the solidified salt inside the microtubes can be dissolved by water.

2.2. Conductive Polymer Preparation. The epoxy resin and hardener (from MAS Epoxies) are mixed at mass ratio of 2:1 as directed, and then a certain amount of carbon black is added into the mixture. The final mixture is cast on a glass slide to make a thin film. After cured for 2 h, conductive copper tapes are attached on the thin film at controlled spacing as electrical contacts. The measured resistances are converted to conductivities by considering the spacing between contacts and the thickness of the polymer film, where the thickness is estimated from the mass and surface area of the film.

2.3. Filling the Microtubes with Polymer Healing Agent. The liquid prepolymer epoxy and its mixtures with carbon powders have shown high viscosities at ambient conditions. The reported viscosity of prepolymer is between 9000 and 10500 mPa s (at 25 °C). The viscosity of prepolymer-carbon black mixture is determined to be similar as that of prepolymer by comparing the times required to flow a certain amount of prepolymer and its mixture through a fixed distance. The mixture of prepolymer and carbon black, and the pure hardener separately filled in glass microtubes by applying vacuum on the other ends of microtubes (a plastic syringe is used for connection of microtube and vacuum pump, vacuum grease is used for sealant), followed by sealing both ends with wax. The time needed to fill one microtube depends on the diameter and length of microtube. It takes 6, 14, and 20 s to fill 10 cm long microtubes with diameter of 600, 450, and 360 μm. The successful filling can be judged by the air-epoxy interface position through the transparent glass tubes.

2.4. Mechanical Property Test. The mechanical properties of individual microtubes before and after filling healing agents are determined by using three point bending measurement. A sheet-shape beam with dimension of 60 × 32 × 2 mm^3 is fabricated for the test. The beam is applied with continuous increasing load until cracks happen. The beam is left curing for 3 h and repeat this load vs displacement test to the same level as previous test in order to evaluated the healing result. The process is repeated 4 times until no crack happens again.

2.5. Self-Reporting Test. A 2 × 2 microtubes network is used to verify the reporting system. One ends of four Cu−P wires inside the microbues are connected to the data acquisition system by measuring the resistance. The epoxy composition is intently damaged at the junctions of perpendicular glass microtubes. As the broken of those tubes, conductive healing agents are released. The resistance changes are recorded to show the healing process and the data acquisition channel will mapping the broken location.

A Hitachi 3500 scanning electron microscope (SEM) is used to characterize the cross sections of this composite and single-wire structure. Digital camera is used to image the 2D sheet structure. An Agilent 34970 data acquisition system is used to measure the resistivity.

3. RESULTS AND DISCUSSION

Figure 2A is a SEM image of an alloy microwire encapsulated in a hollow glass microtube taken at the cross-section direction. The diameter of the alloy microwire is 50 μm, and the thicknesses of outer and inner microtubes are 150 and 200 μm, respectively. The volume fraction of the empty space is derived from these structural parameters as 62%, which determines the amount of healing agents that could be stored in one microtube. Liquid permeation experiment confirms that the long microchannels are hollow from one terminal to the other after dissolving salt.

The total masses of alloy and salt are conserved in fiber drawing, thus the diameters of glass microtube, and spacing between adjacent microwires of alloy or salt will decrease as the length of microfiber increases. To derive the quantitative information of size reduction, we have measured the diameters of microwires and microtubes, the thicknesses of microtubes, and the outer diameters of microfibers. To obtain a set of data, the short tapered piece left after fiber drawing is sliced to plates of different diameter and equal thickness. Each slide is polished and etched to expose microwires and microtubes for measurement. The structural parameters of each microwire or

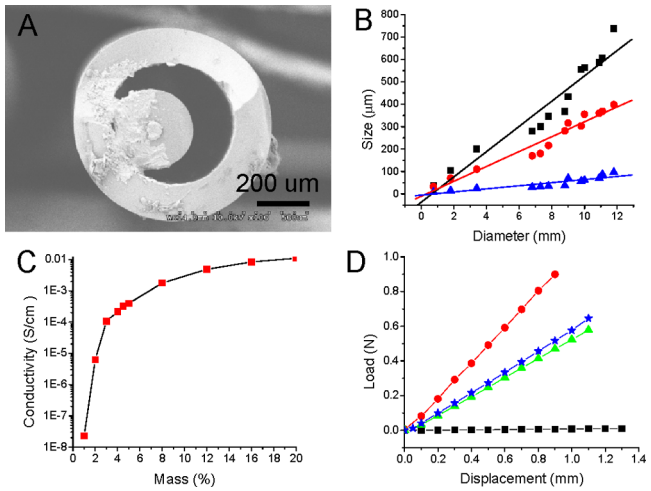

Figure 2. (A) SEM image of a glass microtube with integrated alloy microwire; (B) size scaling of the inner diameter of hollow microtube (square), the diameter of microtube that encloses conductive microwire (circle), and the diameter of microwire (triangle) as the functions of the outer diameter of glass microtube; (C) conductivity of epoxy polymers mixed with various amounts of carbon blacks; (D) the load–displacement curves of a alloy microwire (circle), a hollow glass microtube (star), a microtube filled with solid epoxy polymer (triangle), and an epoxy microrod (square).

microtube are measured as a function of microfiber diameter. Figure 2B demonstrates the size scaling of the inner diameter of hollow microtube (square), the outer diameter of glass tube that encloses conductive microwire (circle), and the diameter of microwire (triangle) as the functions of the outer diameter of microtube. (Note: to obtain sufficient data for size scaling, the fiber drawing is done for a second time on a bundle of first drawn fibers.) The straight lines have different slopes due to the different coefficients of thermal expansion of glass, salt and alloy at fiber drawing temperature. From the slopes of three lines, the ratios of coefficients of thermal expansion have been derived to be 0.86 for the glass-alloy combination, and 0.54 for glass–salt combination. Taking these ratios into account, the inner diameter of outside tube, the outer diameter of inside tube, as well as the diameter of microwire after fiber drawing can be derived from following equations

$$D_1 = \frac{\eta\Phi r_1}{(r_1 + t)},\ D_2 = \frac{\eta\Phi r_2}{(r_1 + t)},\ D_3 = \frac{\eta\Phi r_3}{(r_1 + t)} \quad (1)$$

where Φ, D_1, D_2, and D_3 are the outer diameter of outside tube, inner diameter of outside tube, outer diameter of inside tube and the diameter of microwire after drawing, respectively; r_1 and t are the inner radius and thickness of glass tube before drawing, respectively; η is the ratios of coefficients of thermal expansion for glass–salt or glass–alloy; r_2, and r_3 are the outer radius of inside glass tube, and the radius of alloy powder core prior to fiber drawing, respectively. The minimum diameter of microfiber that can be pulled by a rubber conveyor without breaking is about 250 μm. The alloy microwires are continuous as long as the diameter is over than 10 μm. By changing the parameters of starting glass tubes, the volume available for healing agent can be optimized to contain as much agent as possible, and at the same time maintain the connectivity of alloy microwires.

The percolation threshold of carbon black powders (obtained from Cabot) in polymer (i.e., epoxy) has been determined by measuring the electrical conductivities of polymer–carbon black composites.[30] Figure 2C shows the dependence of conductivity on the mass ratio of carbon black in thin films across a 2 cm distance, where the conductivity increases from 9.1×10^{-8} to 1.8×10^{-3} S/cm as the mass ratio of carbon black increases from 1 to 8%, and the threshold mass ratio is determined to be 3% as the slope of this curve change sharply before this mass ratio. The relative high electrical conductivity is resorted to the excellent dispersion of carbon powders inside the polymer. The carbon powder–polymer composite has uniform color, and does not show regions with large contrasts in SEM images, which reflects its good dispersion. As a comparison we have attempted to use multiwalled carbon nanotubes as conducting phases. Although the high aspect ratio nanotubes could be beneficial to conduct electrons at lower concentrations, the electrical conductivity is too low even at the mass ratio of 10% because of the poor dispersion of nanotubes in liquid prepolymer. In contrast, the carbon black powders can be easily handled and dispersed, and obtained at large quantity at low cost. Adding carbon powders also enhance the fracture resistance behaviors of polymer by pinning motions of dislocation lines. Therefore, carbon black is used as conductive phase inside the polymers at the mass ratio of 3% in the following experiments, which is enough to show the status of cracking and healing processes.

Figure 2D shows the relationship between the applied loads and according displacements of a pure Cu–P microwire (circle), an empty glass microtube with microwire (star), and the same glass microtube filled with epoxy solid (triangle) and an epoxy resin rod (square). Each sample is spanned over a 6 cm gap, where both ends can move freely, and a linearly increasing load is applied on the center of the sample. From the slope of each line, the equivalent Young's moduli of an empty microtube and a glass microtube filled with the epoxy solid are derived as 54.3 and 49.3 GPa, respectively. After polymerization the strength of microtube does not change much because the Young's modulus of epoxy solid is small (2.2 GPa). It has been shown that shape-memory alloy wires can also be incorporated to enhance the mechanical property of polymer.[31] Since the equivalent Young's moduli of Cu–P alloy (92.7 GPa) and glass (54.3 GPa) are larger than that of the polymer (2.2 GPa), the strength of polymer is enhanced after incorporating glass microtubes and alloy microwires.

The glass microtubes can be assembled to form two-dimensional (2D) networks before filling mixtures of carbon black, epoxy and hardener. The packing can be done group-wise where the parallel aligned microtubes are pushed on one side to form a dense layer. Repeating the same action can build the second layer on top of the first one with controlled orientation. After that, a mixture of epoxy resin and hardener at mass ratio of 2:1 is poured on the network to make polymer. Figure 3A shows an optical image of a double-layered microtube network covering an area of 25 × 25 cm^2 with an average intertube spacing of ~300 μm, where carbon blacks are not added to microtubes in order to observe individual microtube. The contrast in the image comes from the light scattering from the inner surface of microtube. The spacing of adjacent microwires determines the spatial resolution in locating damaged point, which is two times the wall thickness of microtube. In an enlarged image (Figure 3B), the orientations of microtubes in two layers are nearly perpendicular to each other. Such orientations simplify the identification of damage in orthogonal coordinate. The

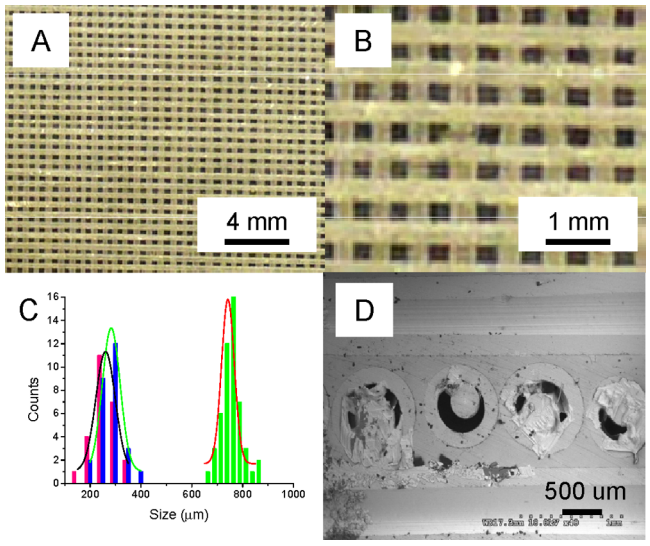

Figure 3. (A) Optical micrograph of a dual-layer microtube network that contains healing agents and covers an area of 25 × 25 cm^2; (B) enlarged image shows orientations of microtubes in the two layers; (C) size distributions of the intertube distances in x (pink bars) and y (blue bars) directions, and diameter (green bars) of microtubes; (D) SEM image taken from the edge of a 2D microtube network.

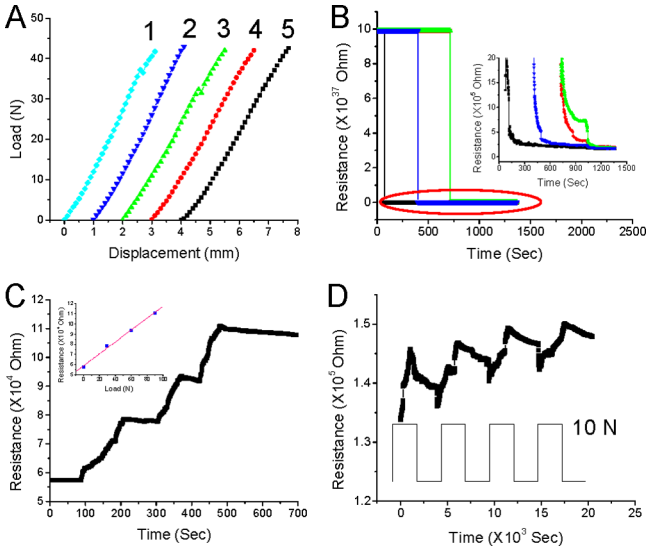

Figure 4. (A) Load–displacement curves before and after damage/healing; (B and inset) resistance changes of four detection nodes after damage/healing process; (C) the resistances across microwires with incremental load of 10 N, and (inset) the relation between resistances and loads; (D) the resistance changes when a 10 N load is applied for 60 min and released.

intertube distances in x and y direction, and diameter of microtubes have shown narrow distributions around 280, 260, and 730 μm, respectively (Figure 3C). Figure 3D shows an SEM image taken from the edge of a polymer with 2D network of microtubes, where the polymer–microtube interfaces can be seen clearly as rings, and the two layers of microtubes are aligned perpendicular to each other. To fill microtubes with hardener or a mixture of carbon black and liquid prepolymer, four sides of composite are polished to expose inlets. The microtubes are filled by immersing one end of polymer–microtube composite into the mixture of carbon black and prepolymer and applying vacuum on the other end. After filling one layer, the second layer of microtubes is filled with hardener using the same method.

We have measured the mechanical properties of a thin polymer sheet (60 × 32 × 2 mm^3) that has an embedded network of microtubes (diameter of 730 μm) containing microwires and healing agents. Figure 4A shows the load–displacement curves obtained from several bending measurements. For pristine sample, crack occurs at load of 37 N with displacement of 2.6 mm (curve 1), where the sudden decrease in load is attributable to the propagation of cracks and delamination above critical level. After healing for 3 h, the load–displacement curve is continuous up to the same load level (curve 2). Repeating the same damage/healing cycle at a different location shows similar trends as shown in curves 3 and 4. Curve 5 shows the strength of the sample does not change after three days. From the slopes of undamaged, damaged and healed samples, their Young's moduli are calculated as 4.0, 2.6, and 3.5 GPa, respectively. In addition, we notice the partial recovery of the mechanical property after healing, which has been attributed to the nonrepairable damage to glass microtube after releasing healing agents. In the original composite, the glass microtubes reinforce the strength of polymer.

Connecting microwires by percolating carbon powders changes the resistances across alloy microwires. In the case of single damage to polymer and sensing network, the resistance change across adjacent microwires has a definite value that is determined by the conductivity, and geometry of the conducting bridge. However, if multiple damages occur sequentially, the resistances measured at different node are related to each other. Taking a 2 × 2 network as a unit, healing the first damaged spot (A_{11}) changes its resistance to R by connecting adjacent microwires. Healing the second (A_{12}) and third (A_{22}) damaged spots reduce their resistances to R as well. But, the resistance at the fourth spot (A_{22}) is $3R$ due to the parallel arrangement of three resistors (A_{11}, A_{12}, and A_{21}). Furthermore, healing the fourth damaged spot (A_{22}) will change four resistances to $3R/4$ shown as theoretical resistances in Table 1. The arrangement of resistors can be extended beyond a unit cell. Generally, for an $m \times n$ array of microwires, if all detection nodes are damaged and healed, the resistance of each spot could be derived from:

$$R_{mn} = \frac{(m+1)}{(m-1)n+2}R \qquad (2)$$

To map the locations of damages on a 2D network, we have used a multichannel data acquisition unit to monitor the resistances across a series of Cu–P microwires. One end of the Cu–P wire is connected to the data logger, and the perpendicular 2D network will form an open-circuit positioning system. Once there is a crack in this system, conductivity healing agent will be released and connect the circuit, an abrupt change of resistance will report the damage of a certain location. The resistance changes after breaking the four points at sequence of A_{11}, A_{22}, A_{22}, and A_{21} are shown in Figure 4B, where the resistances change from infinity to kilo ohms. Figure 4B inset shows the resistance changes in healing process. The resistance reaches stable value in ~300 s, suggesting the completeness of healing process. The stable resistances of four spots are shown in Table 1 as measured resistances. The differences in the measured and theoretical resistances are induced by the variation in the sizes and shapes of percolating chains of carbon powders. Although the differences cannot be

dx.doi.org/10.1021/am3009746 | ACS Appl. Mater. Interfaces 2012, 4, 3759–3764

Table 1. Resistance Changes in the Sequential Breaking of Each Point in a 2 × 2 Matrix

	R_{11} (kΩ)		R_{22} (kΩ)		R_{12} (kΩ)		R_{21} (kΩ)	
sequence	theoretical	measured	theoretical	measured	theoretical	measured	theoretical	measured
	∞	∞	∞	∞	∞	∞	∞	∞
A_{11}	R	251.8	∞	∞	∞	∞	∞	∞
A_{22}	R	212.4	R	267.6	∞	∞	∞	∞
A_{12}	R	186.4	R	241.8	R	323.6	$3R$	729.5
A_{21}	$3R/4$	158.4	$3R/4$	197.0	$3R/4$	174.0	$3R/4$	172.8
R_{avg}[a]		215.45		257.4		277.8		236.8

[a]To derive the average resistance of each resistor (R_{avg}), we multiplied the measured resistances after breaking A_{21} by 4/3; the measured resistance at A_{21} (R_{21}) is divided by 3.

removed due to the unknown effect of damages, the resistance change could definitely reflect the possible locations of damages. Forming an array of larger network could make the measurement difficult by wiring more microwires, but the general principle of resistance changes applies to the whole network. Further deformation to the same location changes resistance by changing percolating path of electrons. Figure 4C shows the resistances across two microwires measured with stepwise increased loads of 10 N. After each increasing, the load is held for tens seconds, the resistance increases as the load increases. Figure 4C inset shows the linear relation between the resistances and the loads. In addition, although the resistance change can only be detected after repairing, it can be utilized reversely to show the magnitude and location of load applied at different time. After releasing the load completely, the resistance decreases slowly as shown in Figure 4D, where 10 N load has been applied for certain time, and then released. After several load cycles, the resistance changes become stable.

To optimize the damage repairing and position sensing, the amounts of healing agents should be maximized, which means the masses of glass and alloy materials should be at minimal level. On the other hand, glass microtubes have to be handled manually and should be broken only when the load is large enough to cause damage to the polymer (exceeding yield strength). Deriving the structure−stress relationship of a microtube with asymmetric cross-section is hard, thus the integrated microtube/microwire structure is treated simply as a microtube (Figure 5A). Such simplification is reasonable because the inner microtube only touches the outside tube on the inner surface. The fracture strength of brittle materials (i.e., glass) is controlled by defects generated in the glass drawing process. It has been shown that the fracture stress of glass can be enhanced greatly by forming a smaller diameter fiber as described in Griffith equation[32]

$$\sigma_f = \sqrt{\frac{2E\gamma}{\pi c}} \tag{3}$$

where σ_f is the stress at the moment of fracture, γ the surface energy of glass (0.047 J/m^2), c is the major axis of an elliptical crack (half crack length), which is generated on the outer surface of microtube during drawing process, and E is Young's modulus determined by the length (L), outer diameter (D), and inner diameter (d) of microtube $E = kL^3/(192I)$ for both-end fixed microtube, where the moment of inertia (I) is $I = \pi(D^4 - d^4)/64$.The eq 3 is then rewritten as

$$\sigma_f = \sqrt{\frac{2kL^3\gamma}{3\pi^2(D^4 - d^4)c}} \tag{4}$$

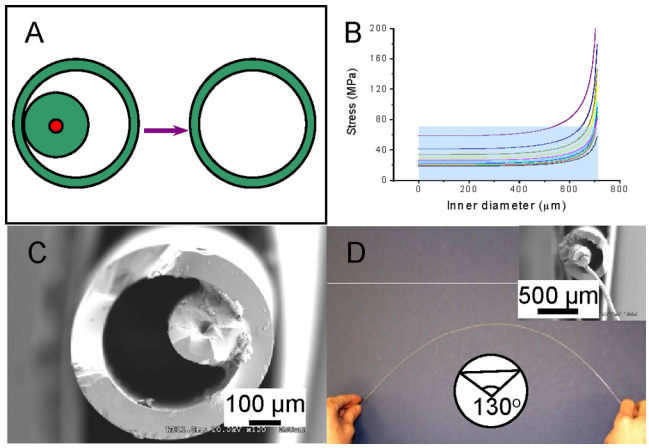

Figure 5. (A) Equivalent microtube structure used to derive the elastic stress of microtube; (B) relation of fracture stress and inner diameter of microtube at different sized initial cracks; (C) glass microtube with the microwire diameter of 20 μm and free volume fraction of 69%; (D) optical image of a curved 50 cm long microtube, where the minimal curvature is 40 cm; (inset) SEM image of a broken microtube with curved alloy microwire.

In the equation, the spring constant is determined to be 141.6 N/m from the load−displacement curve (Figure 2D). For a glass microtube with length of 6 cm and outer diameter of 730 μm, the fracture stress is calculated as the function of inner diameter as shown in Figure 5B, where each curve is collected with half crack length from 0.1 to 1 μm (top to bottom). For the same sized crack, the fracture stress increases as the inner diameter of microtube increases (the tube wall is thinner). If the stress applied on the microtube is larger than a critical value, the glass microtube breaks. Taking the yield strength of epoxy polymer as 71 MPa, the glass microtube with structures shown in the shadow area of Figure 5B should be broken, where the fracture stresses are smaller than 71 MPa. As the size of crack generated in the application of epoxy polymer is more than 100 μm or even at millimeter scale, it is reasonable to assume that the size of crack made in fiber drawing process is around 1 μm. Such small cracks had been used to derive the original fracture theory by Griffith, and confirmed later by electron microscopy.

The diameters and thicknesses of glass microtubes, and the diameter of microwires are controlled by starting glass tubes, and the scaling ratio of the fiber drawing process. A glass tube of 4 cm diameter has been used to make microtubes with diameter of 400 μm, which is restricted by needs to handle microtubes in fiber-drawing and assembling. Providing the same scaling ratio (100) in one draw cycle, the minimal diameter of alloy microwire can be as small as 10 μm by filling a

glass tube with inner diameter of 1 mm. The outer diameter of glass tube is 3 mm, which leaves the thickness of tube of 1 mm. In such case, the ratio of empty space is 69% of the volume occupied by microtube inside polymer. Although the optimized structures have not been made yet due to the limited size choice on commercially available glass tubes, we have shown that it is feasible to make continuous conductive microwires with diameter of 20 μm and length of meters in one draw (Figure 5C). This microwire network-based sensing mechanism depends on the continuities of alloy microwires. At moderate load (70 MPa) that glass microtube breaks, the alloy microwire bends as indicated in Figure 5D inset. The alloy microwire breaks at much higher load (220 MPa), at which the damages to the polymer can be too large to be healed. At last, the microtube encapsulated alloy microwires can be assembled on curved surfaces. Figure 5D is an optical image of a curved microtube, where the minimal curvature is determined as 40 cm. The long and bendable microtubes will enable an intimate coverage on large curved surfaces. To cover an area of 1 m^2 with spatial resolution of 400 μm, 2500 × 2500 microwires with diameters of 400 μm are needed if these microwires are closely packed. In case of high density wire network, line-by-line scan can be utilized in order to monitor the resistances of a large number of detection nodes as what is being practiced in modern display fields.

4. CONCLUSIONS

The direct manipulations of encapsulated alloy microwires to make ordered two-dimensional networks allow the construction of integrated damage repairing and sensing polymer materials based on mimicking the structure and function of biological system. The high precision of coordinately aligned microtubes allows in situ detections of damage/repair events and their locations. The long and flexible microtubes enable the intimate coverage on large and curved surface areas. The detection threshold and the healing capacity can be optimized by changing structures of microtube and microwire. The method depends on low cost materials such as glass, salt, alloy wire, and carbon black, which provides an economic choice. In the full extent of this method, the structural damages to self-healing polymer with embedded microwire sensing network can be displayed in real-time, which will definitely improve reliability and reduces maintenance costs for critical mechanical parts by offering high spatial resolution, efficiency and certainty. Considering the multifunctional piezoelectric materials, the incorporation of such materials into the 2D sensing network would be practiced in the future.[33]

AUTHOR INFORMATION

Corresponding Author

*E-mail: yan.hong@rheem.com.

Notes

The authors declare no competing financial interest.

ACKNOWLEDGMENTS

This work was carried out in materials fabrication lab at NanoScience Technology Center (NSTC) of University of Central Florida (UCF). The microscopy was characterized at Materials Characterization Facility (MCF) at UCF.

REFERENCES

(1) Trask, R. S.; Williams, H. R.; Bond, I. P. *Bioinsp. Biomim.* **2007**, *2*, 1.
(2) Mauldin, T. C.; Leonard, J.; Earl, K.; Lee, J. K.; Kessler, M. R. *ACS Appl. Mater. Interfaces* **2012**, *4*, 1831.
(3) Cho, S. H.; Andersson, H. M.; White, S. R.; Braun, P. V. *Adv. Mater.* **2006**, *18*, 997.
(4) White, S. R.; Sottos, N. R.; Geubelle, P. H.; Moore, J. S.; Kessler, M. R.; Sriram, S. R.; Brown, E. N.; Viswanathan, S. *Nature* **2001**, *409*, 794.
(5) Shchukin, D. G.; Mohawald, H. *Small* **2007**, *3*, 926.
(6) Caruso, M. M.; Davis, D. A.; Shen, Q.; Odom, S. A.; Sottos, N. R.; White, S. R.; Moore, J. S. *Chem. Rev.* **2009**, *109*, 5755.
(7) Yang, J.; Keller, M. W.; Moore, J. S.; White, S. R.; Sottos, N. R. *Macromolecules* **2008**, *41*, 9650.
(8) Tookey, K. S.; Sottos, N. R.; Lewis, J. A.; Moore, J. S.; White, S. R. *Nat. Mater.* **2007**, *6*, 581.
(9) Cho, S. H.; White, S. R.; Braun, P. V. *Adv. Mater.* **2008**, *20*, 1.
(10) Chen, X.; Dam, M. A.; Ono, K.; A., M.; Shen, H.; Nutt, S. R.; Sheran, K.; Wudl, F. *Science* **2002**, *295*, 1698.
(11) Andreeva, D. V.; Fix, D.; Mohwald, H.; Shchukin, D. G. *Adv. Mater.* **2008**, *20*, 2789.
(12) Schniepp, H. C.; Saville, D. A.; Aksay, I. A. *J. Am. Chem. Soc.* **2006**, *128*, 12378.
(13) Canadell, J.; Goossens, H.; Klumperman, B. *Macromolecules* **2011**, *44*, 2536.
(14) Liu, H. A.; Gnade, B. E.; Balkus, K. J. *Adv. Funct. Mater.* **2007**, *18*, 3620.
(15) Wang, H. P.; Yuan, Y. C.; Rong, M. Z.; Zhang, M. Q. *Macromolecules* **2009**, *43*, 595.
(16) McIlroy, D. A.; Blaiszik, B. J.; Caruso, M. M.; White, S. R.; Moore, J. S.; Sottos, N. R. *Macromolecules* **2010**, *43*, 1855.
(17) Caruso, M. M.; Blaiszik, B. J.; White, S. R.; Sottos, N. R.; Moore, J. S. *Adv. Funct. Mater.* **2008**, *18*, 1898.
(18) Yuan, Y. C.; Rong, M. Z.; Zhang, M. Q.; Chen, J.; Yang, G. C.; Li, X. M. *Macromolecules* **2008**, *41*, 5197.
(19) Carlson, J. A.; English, J. M.; Coe, K. J. *Smart Mater. Struct.* **2006**, *15*, N129.
(20) Boller, C. *Smart Mater. Struct.* **2001**, *10*, 432.
(21) Qing, X. P.; Beard, S. J.; Kumar, A.; Hannum, R. *Smart Mater. Struct.* **2006**, *15*, N66.
(22) Wu, D. Y.; Meure, S.; Solomon, D. *Prog. Polym. Sci.* **2008**, *33*, 479.
(23) Zhang, X.; Ma, Z.; Yuan, Z.-Y.; Su, M. *Adv. Mater.* **2007**, *20*, 1310.
(24) Ma, Z.; Ma, L.; Su, M. *Adv. Mater.* **2008**, *20*, 3734.
(25) Ma, Z.; Hong, Y.; Ma, L.; Ni, Y.; Zou, S.; Su, M. *Langmuir* **2009**, *25*, 643.
(26) Hong, Y.; Ma, Z.; Wang, C.; Ma, L.; Su, M. *ACS Appl. Mater. Interfaces* **2009**, *1*, 251.
(27) D'Urso, B. R.; Simpson, J. T.; Kalyanaraman, M. *J. Micromech. Microeng.* **2007**, *17*, 717.
(28) Tonucci, R. J.; Justus, B. L.; Campillo, A. J.; Ford, C. E. *Science* **1992**, *258*, 783.
(29) Donald, I. W. *J. Mater. Sci.* **1987**, *22*, 2661.
(30) Du, F.; Scogna, R. C.; Zhou, W.; Brand, S.; Fischer, J. E.; Winey, K. I. *Macromolecules* **2004**, *37*, 9048.
(31) Kirkby, E. L.; Rule, J. D.; Michaud, V. J.; Sottos, N. R.; White, S. R.; Manson, J.-A. *Adv. Funct. Mater.* **2008**, *18*, 2253.
(32) Dieter, G. E. *Mechanical Metallurgy*. 2nd ed.; McGraw-Hill: New York, 1961.
(33) Lin, Y.; Sodano, H. A. *Adv. Funct. Mater.* **2009**, *19*, 592.